Soft Matter

Three-Dimensional Structures and Symmetry Breaking in Viscoelastic Cross-Channel Flow

Journal:	*Soft Matter*
Manuscript ID	SM-ART-03-2020-000555.R1
Article Type:	Paper
Date Submitted by the Author:	01-Jun-2020
Complete List of Authors:	Qin, Boyang; Princeton University, Mechanical and Aerospace Engineering; Molecular Biology Ran, Ranjiangshang; University of Pennsylvania, Mechanical Engineering and Applied Mechanics Salipante, Paul; NIST Material Measurement Laboratory, Polymers and Complex Fluids Group Hudson, Steven; National Institute of Standards and Technology, Polymers Division Arratia, Paulo; University of Pennsylvania, Mechanical Engineering and Applied Mechanics

Three-Dimensional Structures and Symmetry Breaking in Viscoelastic Cross-Channel Flow

Boyang Qin,[1,2,*] Ranjiangshang Ran,[1] Paul F. Salipante,[3] Steven D. Hudson,[3] and Paulo E. Arratia[1,†]

[1] *Department of Mechanical Engineering & Applied Mechanics, University of Pennsylvania, Philadelphia, 19104, USA*

[2] *Department of Mechanical and Aerospace Engineering, Princeton University, Princeton, 08544, USA*

[3] *Polymers & Complex Fluids Group, National Institute of Standards and Technology, Gaithersburg, 20899, USA*

(Dated: June 4, 2020)

Abstract

Using holographic particle tracking, we report the three-dimensional flow structure organizing the viscoelastic instability in cross-channel flow. Beyond a critical Wi, the advective core flow undergoes an out-of-plane instability marked by the emergence of tertiary flow, resembling that of the toroidal vortices in Taylor-Couette geometry. The out-of-plane flow component distorts the separatrix between the impinging inflow streams, triggering symmetry breaking *normal* to the extension plane. As extensional rate increases, progressively higher order modes of the separatrix are observed, akin to Euler buckling of a rigid column. The disturbances propagate upstream via stress fluctuations despite viscous dissipation. These complex flow structures may be generic to elastic turbulence in mixed flows.

* bqin@princeton.edu

† parratia@seas.upenn.edu

The presence of even minute amounts of polymer can significantly affect the flow of a viscous liquid. At negligible fluid inertia, viscoelastic fluids that are subject to the correct flow gradients and curvature can exhibit hydrodynamic instabilities [1–5] and even turbulentlike flow – dubbed elastic turbulence [6–9]. Similar to the complex routes to turbulence at high Reynolds number, the early stages of elastic turbulence are marked by the emergence of purely elastic instabilities and non-trivial flow structures that are inherently three-dimensional (3-D). For example, in the classic work on the Taylor-Couette flow of polymeric fluids, azimuthal toroidal vortices and rolls emerge beyond a critical rotation speed and are observed to organize the unsteady chaotic flow [1]. Subsequent investigations in other geometries revealed wake vortices behind cylinders [10], chaotic swirls in the flow between parallel plates [6], three-dimensional upstream vortices [11], and spanwise modulations resembling traveling waves [12–14]. Effect of small quantity of polymer on the inertial vortex instability in cross-channel flow is investigated in [15]. While these flow structures may be widely present and are critical in organizing the subsequent chaotic flow, the mechanism of interaction between various modes of instability in the full 3-D space and how they give rise to complex flow patterns and dynamics is largely unknown. With few exceptions, the lack of experimental measurements of these 3-D flow structures hinders our understanding of the nature of this important class of flow.

A prime example of such complexity – both in time and space – is the cross-channel flow. Widely used as a model system to study polymer extension dynamics[16–18] and bulk extensional rheology [19, 20], the cross-channel is a mixed-type flow consisting of curvilinear streamlines separated by the central hyperbolic points. In the purely elastic regime, streamline curvature amplifies secondary flow disturbance [2, 21] in the core flow, while hyperbolic points efficiently stretch polymers and generate large polymer stresses (as seen in birefringence) along the separatrix (unstable manifold) [19, 22, 23]. As a result of such complex flow landscape, the viscoelastic cross-channel flow undergoes a series of hydrodynamic instabilities at large enough strain rates. Experiments using micro-machined cross-channels and viscous polymeric fluids found two flow transitions: a steady symmetry breaking instability in the extensional x-y plane, followed by an unsteady flow switching instability[24]. The mechanism of the instability is attributed to the abrupt polymer stretching near the hyperbolic point. Subsequent 2-D simulations using upper-convected Maxwell model found qualitative agreement with the first steady supercritical transition[25], while simulations us-

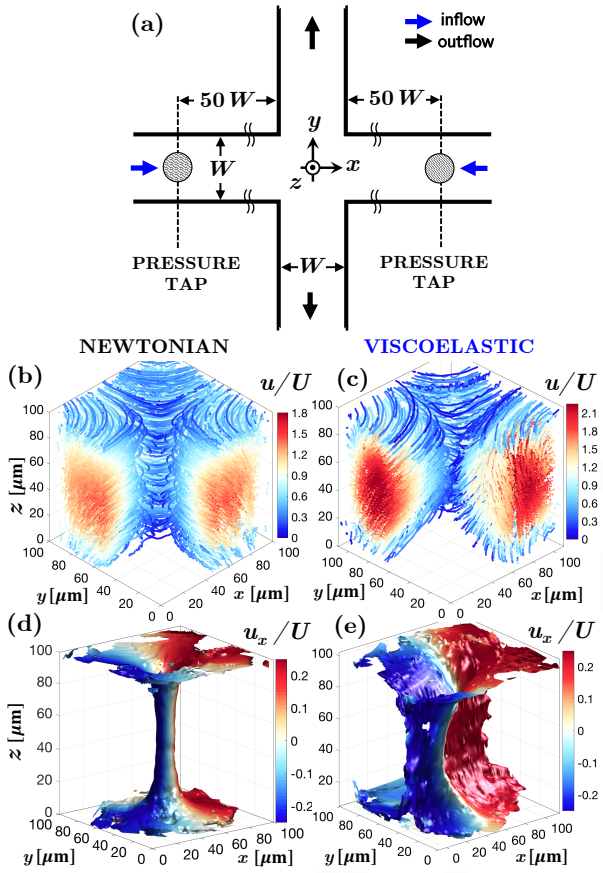

FIG. 1. (a) Schematic of the cross-channel setup. (b,c) Cutaway view of the ensemble of three-dimensional particle trajectories from the holographic tracking velocimetry for (b) Newtonian and (c) viscoelastic fluid at $\dot{\epsilon} = 10\ \mathrm{s}^{-1}$. (d,e) Corresponding isosurfaces with $u/U = 0.3$ (low speed zone) colored by u_x component.

ing FENE-P model identified the oscillatory instability[26]. Recent 3-D simulations of the cross-channel flow argues that the symmetry breaking in extensional plane offers a path of least resistance and reduces the overall drag [27]. The authors reported the occurrence of 3-D velocity components and bifurcation of the hyperbolic points normal to the x-y plane. Such components are observed for finite aspect ratio channels even at vanishingly low Wi (≈ 0.001) and when the flow is symmetric in the extensional plane, which suggests that the base viscoelastic flow is inherently 3-D and 2-D measurements misses the full flow dynamics especially in the turbulent regime. To date, however, it remains unclear what is the relationship between the curved streamline instability and the stress amplification along the separatrix manifold and hyperbolic points. The flow structure and mechanism that organizes the observed instabilities in viscoelastic cross-channel flow is missing.

Here, using time-resolved holographic particle tracking, we report the three-dimensional flow structure that links the curved core flow and the separatrix containing the hyperbolic points. We find that, beyond Weissenberg number unity, the advective inflow undergoes an instability perpendicular to the x-y extension plane marked by the emergence of weak tertiary velocity component u_z, resembling that found in the toroidal vortices in Taylor-Couette geometry. Second, the presence of the out-of-plane flow components then distorts the separatrix manifold (unstable manifold), which undergoes a symmetry breaking instability in the z direction, separate from the symmetry breaking in the 2D x-y plane. As flow rate increases, higher order mode shapes of the separatrix are observed, akin to the buckling of a rigid column under compression, except that here, the origin of the instability is the velocity modulations in the wall-normal z direction arising from normal stress imbalance. Lastly, pressure measurements show that, contrary to the birefringent strands located at the separatrix (unstable manifold)[19, 22], stress disturbances can also propagate far upstream in the direction of the stable manifold, despite viscous dissipation.

The cross-channel used in the experiments has a square cross section with equal width and depth $W = H = 100$ μm, shown in Fig. 1(a). The mean flow velocity is $U = Q/WH$ where Q is the volumetric flow rate prescribed externally by a syringe pump (Harvard Apparatus PHD2000). The polymeric fluid consists of $c = 300\,\mu$g/g polyacrylamide (PAA $18{\times}10^6$ Da) in 90% mass fraction glycerol aqueous solution, with a nearly constant viscosity of approximately $\eta = 0.30$ Pa·s (see Supplemental Information (SI) for rheology [28]). The PAA polymer overlap concentration (c^*) is approximately 350 μg/g [29], or $c/c^* = 0.86$. A Newtonian fluid of 90 wt% glycerol in water is also used for comparison. The Reynolds number is kept below 0.01 for all flow rates used, where $\mathrm{Re} = \rho UW/\eta$ and $\rho = 1.23$ g/cm^3 is the fluid density. The nonlinearity of the polymer conformation can be described by the extensional Weissenberg number, $\mathrm{Wi} = \lambda\dot{\epsilon}$ where the dominant extensional relaxation time is around $\lambda \approx 0.28$ s (as measured by capillary thinning, see SI [28]) and the extensional rate is estimated by $\dot{\epsilon} = 2U/W$.

Three-dimensional particle trajectories, which are used to generate 3-D flow fields, are obtained using holographic particle tracking [30, 31]. The seeded fluid (1 μm dia. tracers, 10^{-5} mass fraction) is illuminated using a laser beam (532 nm) mounted on an inverted microscope and recorded with high speed camera (6000 fps). The out-of-plane (z) positions of tracer particles are obtained using back-scatter reconstruction [11]. Particle trajectories

within a cubic volume (100 μm in width) at the center of the cross-channel are measured. An cutaway view of the the ensemble Lagrangian trajectories are shown in Fig. 1(b), as colored by particle speed. To monitor disturbance propagation, pressure taps are installed $50W$ upstream from the cross-channel center. Signals from both streams are recorded simultaneously (5 ms and 100 Pa resolution), separate from velocimetry measurements.

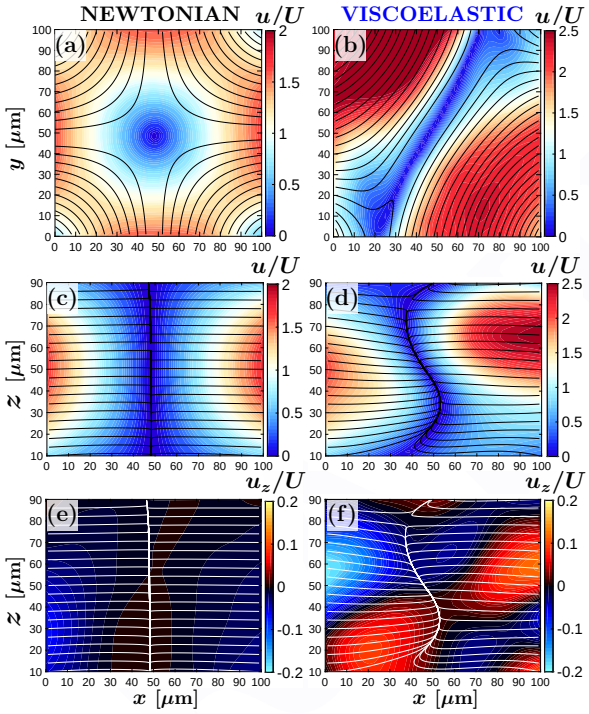

FIG. 2. Cross-sectional velocity maps show planar and tertiary instabilities at $\dot{\epsilon} = 10$ s^{-1} (Wi = 3). Left panel is Newtonian fluid and right is viscoelastic. (a,b) Streamlines and normalized local velocity magnitude u/U, in the extensional x-y plane, showing the well-known planar asymmetric flow instability. (c,d) The same plot in the x-z cut-plane, normal to the extensional plane and along the inflow direction ($y = 50$ μm) Note that the flow enters along x axis and exits along y. (e,f) Normalized tertiary velocity u_z in the same cut-plane.

We begin with the raw particle trajectories within the cubic observation window of the cross-channel at high extension rates. Fig. 1(b,c), show the cut-away views of the ensemble of Lagrangian trajectories for the Newtonian and viscoelastic fluids, where incoming streams approach the cross flow center along the x axis. In contrast to the Stokesian and symmetric flow for the Newtonian fluid in Fig. 1(b), the viscoelastic flow is highly assymmetric between the inflow and outflow streams. The core flow of the viscoelastic fluid also has higher

normalized peak velocity, supporting the view that the symmetry breaking within the plane of extension is redirected via paths of least resistance [27]. The striking difference between the Newtonian case and the viscoelastic case, however, is revealed by plotting the low-speed ($u/U = 0.3$) iso-surface in Fig. 1(d,e), obtained by sectioning the volumetric velocity data from the holographic velocimetry technique. Here, u is magnitude of the local velocity vector. For the Newtonian flow (Fig. 1d), the low speed region takes the form of an axisymmetric cylinder. The inflow streams, distinguished by u_x velocity component (red and blue in Fig. 1d), split around a planar separatrix in the y-z plane, where u_x is close to zero. The viscoelastic case in Fig. 1(e) however, shows a much different structure: the separatrix between the two impinging streams become curved and displays a clear loss of symmetry normal to the plane of extension flow.

The three-dimensional flow structure underlying the instability can be dissected by the cross-sectional velocity maps of the core advective flow. The velocity map within the extensional x-y plane passing the center of the cross-channel is shown in Fig. 2(a,b), where streamlines are overlaid on speed maps u/U. The impinging streams enter along x-axis and exit along y and the flow extensional strain rate is high $\dot{\epsilon} = 10$ s^{-1}. For Newtonian fluid, the flow remains steady and symmetric around the hyperbolic points for all flow rates, as in Fig. 2(a). The flow for the viscoelastic fluid, on the other hand, becomes highly asymmetric and the inflow streams preferentially choose between two bistable outflow directions, as previously documented in experiments [24] and simulations [25, 27]. For our system, the asymmetric flow becomes unsteady and switches between the two bi-stable modes for $\dot{\epsilon} \gtrsim 4$ s^{-1}. We note that, the viscoelastic case under the same volumetric flow rate, is able to achieve higher core flow speed.

The flow structures *normal* to the x-y plane, however, reveal a different landscape for the viscoelastic flow at high strain rate. Figure Fig. 2(c) shows the flow speed on a vertical cross section along x for the Newtonian fluid. As expected, the viscous Stokesian flow has a high degree of left-right symmetry as well as a classic parabolic profile along z-axis, due to the lack of inertia in our system. The viscoelastic fluid at identical strain rate however, sees a completely different picture in Fig. 2(d). The left-right inflow streams no longer mirror each other and the parabolic core flows become shifted in opposite direction in z, leading to a symmetry breaking normal to the plane of extension. Further, the lost of symmetry is accompanied by the emergence of tertiary z velocity component – shown in Fig. 2(f)– that

is absent in the Newtonian case Fig. 2(e). These out of plane velocities are strong (reaching above 10% average flow speed) and resemble the appearance of azimuthal rolls obeserved in a mass-conserved Taylor Couette flow [1]. The out-of-plane velocity component emerges and increases in strength as strain rate increases (SI Fig. 5), in qualitative agreement with [27]. Yet due to the rapid decay of streamline curvature in the cross-channel, these vortices will be spatially localized.

Further, the onset of tertiary instability of the core flows completely alters the unstable manifold associated with the hyperoblic point. As the left-right inflows compete in the out of plane z direction, the separatrix dividing these core flows becomes unstable. It loses left-right symmetry in z and appears to "buckle" with waveforms similar to the bifurcation modes of an Euler column under compressive load, as shown in Fig. 2(f). The waveforms here, however, are unsteady and switch stochastically as the core flow fluctuates in time. The snapshots of the first-order instability modes are shown in Fig. 3(a,b), where the streamwise u_x velocity is normalized by the local speed u. The x-z cross section here passes through the geometric center of the cross-channel and the separatrix is where the inflow x component decays to zero. This fixed observation plane is chosen to represent the separatrix profile to ensure consistency of separatrix profiles between measurements in the unsteady flow. As the flow rate increases, higher order modes are excited and increases in occurance in addition to the low order modes. Figure 3 (c,d) show the second order modes.

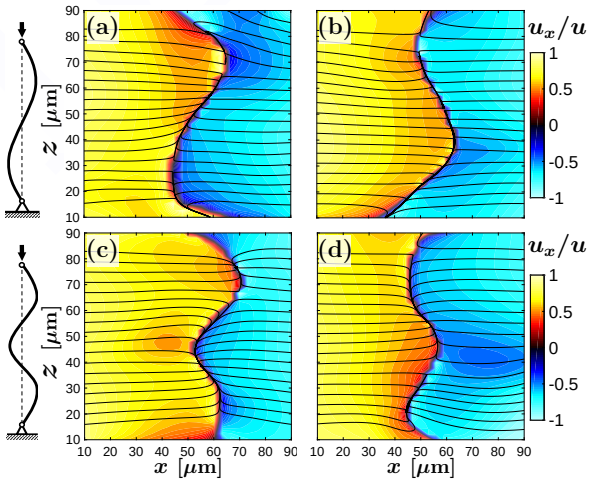

FIG. 3. Instability modes of the separatrix between the two impinging inlet streams at $\dot{\epsilon} = 15\ \mathrm{s}^{-1}$. This boundary undergoes irregular transitions between various shape modes: (a,b) show a second order mode while (c,d) show a third order mode.

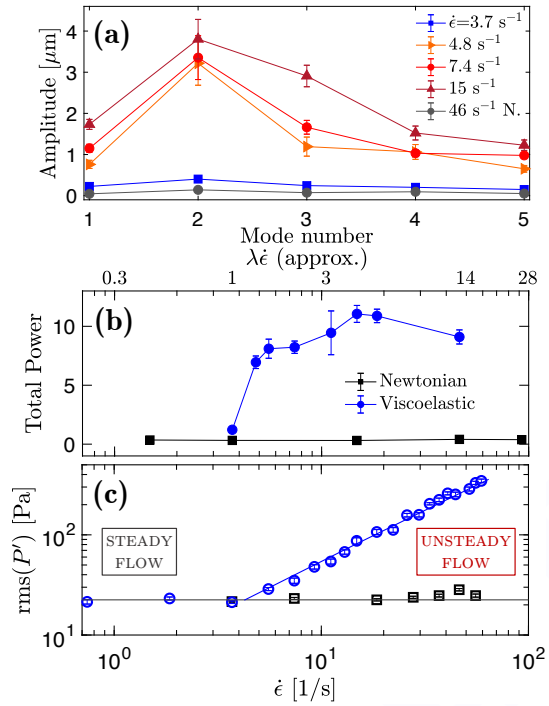

FIG. 4. (a) Statistical mean amplitudes of the instability waveforms, uncertainties from standard deviations of bootstrapped sample mean. (b) The sum of mean amplitudes of first 5 modes as a function of strain rate. Transition from flat to curved separatrix between the two streams occurs at around a critical strain rate of $\dot{\epsilon}_c \approx 4\ \mathrm{s}^{-1}$ or $Wi_c \approx 1.1$. (c) Root mean square pressure fluctuations upstream of the cross-channel show the onset of flow fluctuation occurs at strain rate of $4\ \mathrm{s}^{-1}$.

We can quantify the onset of the instability modes and symmetry breaking in the z direction by measuring the amplitude of each instability mode. We define the amplitude of the n^{th} mode as the integral dot product with the orthogonal sinusoidal modes:

$$A_n = \left| \int_0^H y^* \sin(n\pi y^*/H)\, dz \right|, \qquad n = 1, 2, 3, \ldots \tag{1}$$

where $y^*(z)$ is the profile for the separatrix. This amplitude can be averaged over all observed samples (∼500 individual realizations from 3-D velocity field) and the first five modes are shown in Fig. 4 (a) for various extensional rates. For Newtonian flow at high strain rates (gray curve), the flow is steady and all mode amplitudes are close to zero on par with system noise level. The viscoelastic flow at low extensional rates is similar to the Newtonian case, without mode excitation. Once the extensional rate exceeds $\dot{\epsilon} \gtrsim \dot{\epsilon}_c$, however, a sudden onset of instability modes occurs. The amplitudes increase markedly for all modes. The dominant

mode is the second mode and its strength is relatively independent of Wi. By contrast, the higher order modes saw clear increase in strength, relative to the second mode, as Wi number increases. This indicates increasing excitation of the higher order modes.

The onset of the transition can be captured by the summed average mode amplitude of the first 5 instability modes, plotted in Fig. 4 (b). As extensional rate increases, the Newtonian total amplitude remains close to zero as expected. For the viscoelastic fluid, however, the total mode power transitions to a branch with high level of mode amplitudes at around a critical strain rate of $\dot{\epsilon}_c \approx 4\ \mathrm{s}^{-1}$ or an extensional Weissenberg number of $\mathrm{Wi}_c \approx 1.1$, where the separatrix transitions from flat to curved. The total mode amplitude then saturates for $\dot{\epsilon} > 15\ \mathrm{s}^{-1}$.

The instability in separatrix waveforms and loss of symmetry in z occurs at a critical extensional rate $\dot{\epsilon}_c$ that coincides with the onset of flow unsteadiness. In Fig. 4 (c) the root mean square (rms) of pressure fluctuations $P' = P - \langle P \rangle$ is shown as a function of extensional rate. First, the rms fluctuation for the Newtonian fluid remains constant ($\sim$20 Pa) for all $\dot{\epsilon}$. This level of fluctuation is also similar to the viscoelastic flow in unperturbed straight channel (without cross flow). The viscoelastic case, on the other hand, sees significant increase in pressure fluctuations for $\dot{\epsilon}_c \approx 4\ \mathrm{s}^{-1}$, the onset of unsteady flow in our system. This also corresponds to the approximate strain rate below which, the mode amplitude is not measurable, i.e. close to Newtonian level and system noise. We also note that near the onset of unsteady flow, the characteristic period of the flow switching diverges, see SI Fig.6.

The mechanism for the onset of secondary velocity components in the core flow is analogous to the development of classic toroidal rolls in the curvilinear Taylor-Couette flow[1], except that the streamline curvature is produced by the 90° bend from inflow to outflow. Beyond a critical flow rate and a sufficiently large streamline curvature produced by the bend around the cross-channel center, secondary hoop stresses, from normal stress imbalance, lead to azimuthal toroidal flow cells, arranged along the z axis. At higher flow rates, finer wavelengths of the rolls and hence higher order separatrix modes can be observed[1].

We have shown that the onset of separatrix instability coincides with the onset of pressure fluctuations. Yet the temporal dynamics associated with the complex flow structures observed in the cross-channel, and whether such distance can propagate throughout the flow domain remained unknown. Next, we report evidence that the flow disturbance originating at the cross-channel can induce chaotic fluctuations spanning many timescales and

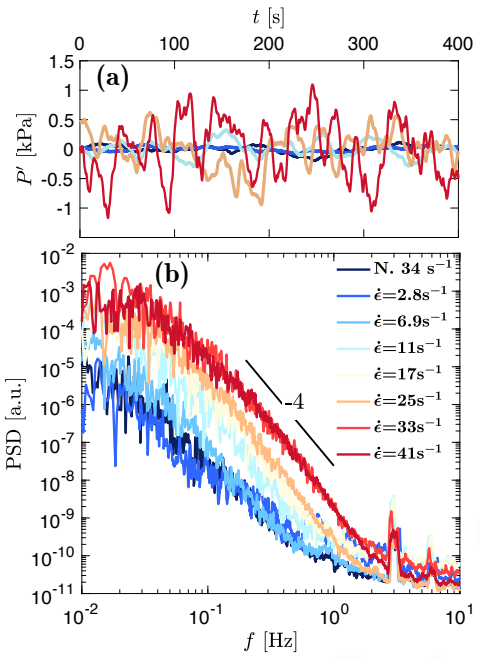

FIG. 5. (a) Pressure signals measured upstream of the cross-channel show large irregular fluctuations for viscoelastic fluids at high extension rates $\dot{\epsilon} \gtrsim 4$ s^{-1}. (b) Power spectra of pressure fluctuations for the corresponding extensional rates.

can propagate far upstream. Birefringence measurements showed that the region of high polymer stretching contains the hyperbolic points and aligns downstream along the unstable manifold [19, 22]. However, in light of recent observations of elastic waves propagating against the mean flow [11, 32], the question arises whether such stress disturbance remains localized near the hyperbolic points. To investigate this, we measured pressure signals $50W$ upstream of the cross-channel center. Figure 5(a) shows that for the viscoelastic fluid at low strain rates $\dot{\epsilon} \lesssim 4$ s^{-1}, the pressure is comparable to the system noise (black, Newtonian $\dot{\epsilon} = 34$ s^{-1}). As the viscoelastic flow rate increases beyond the critical $\mathrm{Wi}_c \approx 1$, however, large pressure fluctuations P' are observed. At $\dot{\epsilon} = 33$ s^{-1} (red in Fig. 5 a), the amplitude of the viscoelastic fluctuations is 20 times the Newtonian counterpart. Our previous work showed that the fluctuations in *velocity* decay rapidly upstream of the flow perturbation, and reduces to the unperturbed system noise level in about $12W$ for flow around a single cylindrical obstable [11] and fluids similar to that used here. In contrast, the fluctuation in pressure and elastic stresses persist much farther upstream.

Further, the irregular pressure fluctuations are activated at many time scales. Figure 5 (b) shows the power spectra of pressure fluctuations. A power law decay in the frequency

(f) power spectrum is observed $f^{-\alpha}$, reaching a fully developed scaling of $\alpha = 4$ for $\dot{\epsilon} \gtrsim 33$ s^{-1}. The decay law here ($\alpha \gtrsim 3$) is characteristic of elastic turbulence, yet steeper than that of pressure signal spectra (f^{-3}) measured experimentally in elastic turbulence in a parallel swirling flow [33]. It is also slightly higher than the power law ($f^{-3.5}$ to f^{-4}) obtained from axial velocity fluctuations $1W$ downstream of the cross-channel outlet from experiment with channel aspect ratio similar to that used here [8]. We hypothesize that power f^{-4} upstream of the hyperbolic region is steeper since energies at higher frequency are more prone to damping compared to those at lower frequencies, similar to the spatial transition found in the velocity power spectra in parallel channel flow[9]. Modeling and experiments of entrance flow of shear banding wormlike micelle fluids, a system dominated by low frequency pressure and velocity fluctuations, suggest that f^{-4} decay may arise from two-sided exponential pulses of random durations [34].

Elastic turbulence in mixed-type flows, consisting of shearing by curvilinear flow and stretching via hyperbolic regions, are widely seen in many systems such as jets, T-junctions, and flow around obstables. Using holographic particle tracking, we identified the 3-D flow structures that underly the transition and early stages of elastic turbulence in a model mixed flow type system. We find that the onset of out-of-plane velocity components in the core flow directly cooperates with the tertiary symmetry breaking and apparent "buckling" of the separatrix waveforms associated with the hyperbolic point. Analogous to the reduction in wavelength in viscoelatic Taylor-Couette flow, fine scales and higher order modes occur. Such complex structures situate normal to the extensional x-y plane and ellude simple planar measurements. Our results imply a generic pathway by which transition to elastic turbulence can occur in mixed flow systems.

We thank B. Thomases and R. Poole for fruitful discussions. P.E.A., B.Q. and R.R. acknowledge NSF CBET-1336171 and S.D.H. and P.F.S. thank NIST-on-Chip funding.

[1] R. G. Larson, E. S. G. Shaqfeh and S. J. Muller, *J. Fluid Mech.*, 1990, **218**, 573–600.

[2] P. Pakdel and G. H. McKinley, *Phys. Rev. Lett.*, 1996, **77**, 2459–2462.

[3] L. Rodd, J. Cooper-White, D. Boger and G. McKinley, *J. Non-Newtonian Fluid Mech.*, 2007, **143**, 170–191.

[4] N. Hoda, M. R. Jovanovi and S. Kumar, *J. Fluid Mech.*, 2008, **601**, 407–424.

[5] M. S. Oliveira, P. J. Oliveira, F. T. Pinho and M. A. Alves, *J. Non-Newtonian Fluid Mech.*, 2007, **147**, 92–108.

[6] A. Groisman and V. Steinberg, *Nature*, 2000, **405**, 53–55.

[7] A. Groisman and V. Steinberg, *New J. Phys.*, 2004, **6**, 29.

[8] P. Sousa, F. Pinho and M. Alves, *Soft Matter*, 2018, **14**, 1344–1354.

[9] B. Qin and P. E. Arratia, *Phys. Rev. Fluids.*, 2017, **2**, 083302.

[10] G. H. McKinley, R. C. Armstrong and R. A. Brown, *Proc. R. Soc. A*, 1993, **344**, 265–304.

[11] B. Qin, P. F. Salipante, S. D. Hudson and P. E. Arratia, *J. Fluid Mech.*, 2019, **864**, R2.

[12] D. Bonn, F. Ingremeau, Y. Amarouchene and H. Kellay, *Phys. Rev. E*, 2011, **84**, 045301.

[13] L. Pan, A. Morozov, C. Wagner and P. E. Arratia, *Phys. Rev. Lett.*, 2013, **110**, 174502.

[14] B. Qin, P. F. Salipante, S. D. Hudson and P. E. Arratia, *Phys. Rev. Lett.*, 2019, **123**, 194501.

[15] N. Burshtein, K. Zografos, A. Q. Shen, R. J. Poole and S. J. Haward, *Phys. Rev. X*, 2017, **7**, 041039.

[16] T. T. Perkins, D. E. Smith and S. Chu, *Science*, 1997, **276**, 2016–2021.

[17] D. E. Smith and S. Chu, *Science*, 1998, **281**, 1335–1340.

[18] C. M. Schroeder, H. P. Babcock, E. S. G. Shaqfeh and S. Chu, *Science*, 2003, **301**, 1515–1519.

[19] S. J. Haward, M. S. Oliveira, M. A. Alves and G. H. McKinley, *Phys. Rev. Lett.*, 2012, **109**, 128301.

[20] S. J. Haward, G. H. McKinley and A. Q. Shen, *Sci. Rep.*, 2016, **6**, 33029.

[21] R. Larson, *Rheol. Acta*, 1992, **31**, 213–263.

[22] G. G. Fuller and L. G. Leal, *Rheol. Acta*, 1980, **19**, 580–600.

[23] S. J. Haward, *Rheol. acta*, 2010, **49**, 1219–1225.

[24] P. E. Arratia, C. C. Thomas, J. Diorio and J. P. Gollub, *Phys. Rev. Lett.*, 2006, **96**, 144502.

[25] R. J. Poole, M. A. Alves and P. J. Oliveira, *Phys. Rev. Lett.*, 2007, **99**, 164503.

[26] L. Xi and M. D. Graham, *J. Fluid Mech.*, 2009, **622**, 145–165.

[27] F. Cruz, R. Poole, A. Afonso, F. Pinho, P. Oliveira and M. Alves, *J. Non-Newtonian Fluid Mech.*, 2016, **227**, 65–79.

[28] *Supplementary Information*.

[29] E. Pelletier, C. Viebke, J. Meadows and P. Williams, *Langmuir*, 2003, **19**, 559–565.

[30] F. C. Cheong, B. J. Krishnatreya and D. G. Grier, *Opt. Express*, 2010, **18**, 13563–13573.

[31] P. F. Salipante, C. A. Little and S. D. Hudson, *Phys. Rev. Fluids*, 2017, **2**, 033302.

[32] A. Varshney and V. Steinberg, *Nat. Commun.*, 2019, **10**, 652.

[33] Y. Jun and V. Steinberg, *Phys. Rev. Lett.*, 2009, **102**, 124503.

[34] P. F. Salipante, S. E. Meek and S. D. Hudson, *Soft Matter*, 2018, **14**, 9020–9035.